Bulletin of Earthquake Engineering (2019) 17:1739–1762
https://doi.org/10.1007/s10518-018-0494-6

ORIGINAL RESEARCH

Seismic performance enhancement of high-voltage post insulators by a polyurethane spring isolation device

Tansu Gökçe[1] · **Ercan Yüksel**[2] · **Engin Orakdöğen**[2]

Received: 9 February 2018 / Accepted: 8 October 2018 / Published online: 11 October 2018

Abstract
High-voltage (HV) post insulators are vulnerable components of the electrical substations during strong earthquakes. It is rather hard to repair them in service. There are two controversial approaches to increase their seismic safety. They are application of the base stiffening techniques and utilization of the base isolation systems. A new low-cost seismic isolation device that is mounted underneath of HV post insulator is being proposed here to provide period elongation and supplementary damping. The seismic isolator consists of two steel plates, four polyurethane springs and a steel rod. Its cost is insignificant compared with price of HV post insulator. Quasi-static and shake table tests were performed on fixed base and isolated specimens. A set of historical acceleration records selected according to IEEE-693 were utilized in the dynamic tests. The supplementary damping provided by the isolation system was determined between 4 and 8%. The accelerations as well as base shear and base moment of HV post insulator were reduced about 20–70% thanks to the isolation system. The generated numerical models reproduced the experimental results. Consequently, the isolation system is capable to enhance the seismic safety of HV post insulators.

Keywords Earthquake safety · Seismic isolation · Low-cost isolation · Post insulator · Polyurethane spring

1 Introduction

HV post insulators are vulnerable components of electrical substations. They might be heavily damaged in strong earthquakes. It is difficult to repair those damages without removing the post insulators from the service. The replacement costs as well as indirect costs due to interruption of the power supply are somewhat significant. In 1994 Northridge-America, 1995 Kobe-Japan, 1999 İzmit-Turkey and 1999 Chi–Chi-Taiwan Earthquakes, the losses were hundreds of millions of dollars for each event. Damage of the electrical substation equipment in Loma Prieta and Northridge Earthquakes resulted $283,000,000 worth of losses (Schiff 1998).

✉ Ercan Yüksel
yukselerc@itu.edu.tr

[1] Institute for Science and Technology, Istanbul Technical University, Maslak, Istanbul, Turkey

[2] Faculty of Civil Engineering, Istanbul Technical University, Maslak, Istanbul 34469, Turkey

The observed damages during earthquakes are generally concentrated nearby the base connection (Gokce et al. 2018). Two distinct failure modes of the porcelain insulator are illustrated in Fig. 1. Dependently, it will be useful to reduce the internal forces at the bottom to increase the seismic safety.

Hatami et al. (2004) performed several shaking table tests to determine seismic performance of the transformer and its insulator. The results of the shaking table tests were utilized to develop the analytical models for different height and stiffness cases. It was introduced some comments to decrease collapse probability, and some retrofitting procedures. Murota et al. (2006) performed tri-axial shaking table tests of the power transformers for two isolation systems. They were sliding bearings combined with rubber and the segmented high damping rubber bearings. The interaction between bushing connecting cables and the bushing in the base-isolated system was experimentally studied. They stated that the base isolation when properly designed is very effective for seismic protection of power transformers even in existence of the connection cables. Kong and Reinhorn (2009) performed shake table tests of the full scale disconnect switch with supporting structure. Two dissimilar base isolation systems, friction pendulum and wire rope systems that were located under the supporting structure were utilized to reduce seismic risk of the insulators. The friction pendulum system decreased the demand parameters of the post insulators by 50–90%. Koliou et al. (2009) proposed a stiffening technique to reduce the seismic demand. They stated that the flexural stiffeners placed on the top plate of the transformer structure reduced the seismic action and improved seismic behavior of the transformer bushing system.

Alessandri et al. (2015a, b) accomplished a contemporary study in Europe. They proposed a seismic isolation system made of wire ropes for HV circuit porcelain breakers. It was concluded that wire ropes reduced maximum stress of ceramic about 75%. Therefore, seismic safety of the porcelain breakers was increased enormously. Takhirov et al. (2017) proposed a similar base isolation system, also. Based on the performed system tests, they concluded that the isolation device reduced the seismic demands by a factor of 2.5.

Lee and Constantinou (2018) developed and tested the combined horizontal-vertical seismic isolation system for high-voltage–power transformers. The system consists of triple friction pendulum isolators to provide horizontal isolation. They were supported by coil steel springs, linear viscous dampers and the telescopic system. The tests demonstrated effectiveness in significantly reducing the horizontal accelerations in all cases, and in reducing the vertical accelerations in some cases. There were exceptions in which vertical

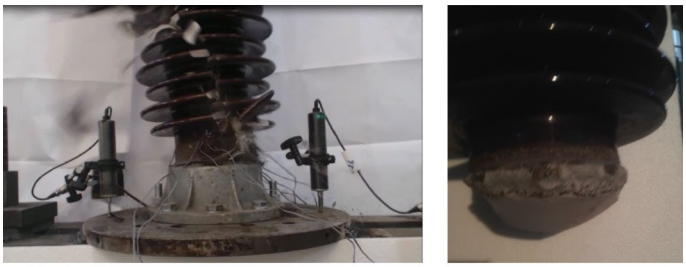

a **b**

Fig. 1 Two different failure modes of porcelain insulators (courtesy of Tansu Gökçe). **a** Shear failure, **b** flexural failure

input acceleration was unreduced or slightly magnified in vertical direction in the cases of motions with strong vertical spectral components at frequencies about 2 Hz.

IEEE-693 (2006) defines seismic testing and qualification of the substation equipment. It defines three performance levels namely high, moderate and low according to the importance and voltage range of the members. It requires experimental works to attain moderate and high performance levels. Two percent of damping ratio is recommended for analysis of porcelain post insulators. In addition, it states that if the equipment is tested without the supporting system, the input acceleration to be used in the shake table should be amplified by a factor. Villaverde et al. (2001) performed some tests on 230-kV and 500-kV transformers. Although the amplification factors were determined less than 2.0 alike IEEE-693 suggestion for 500-kV bushings, they were about 3.95 that is almost double of IEEE-693 suggestion for 230 kV bushings. Filiatrault and Matt (2006) investigated dynamic response of porcelain bushings mounted on the transformer tanks. They indicated that dynamic properties of the bushings mounted on flexible support are significantly different from that of the same bushings mounted on the rigid base. They stated that the amplification factor suggested by IEEE-693 might not be conservative for all bushing systems. Whittaker et al. (2004) performed shake table tests for 196-kV, 230-kV and 550-kV insulators. They evaluated the fragility test procedure according to IEEE-693. They stated that fragility data based on the spectral acceleration at predominant frequency of insulator provides an improved estimate of damage but cannot account substructure flexibility and damping. Both of which may intensely affect bushing response.

Polyurethane elastomers have been utilized in various applications such as rollers, suspension pads, industrial belts etc. The chemical resistance of polyurethanes allows them to be used extensively in the industry, (Clemitson 2015).

Buckle et al. (2006) made a publication to present principles of the existing seismic isolation systems for highway bridges and their seismic analysis methods. The study combines lead rubber, friction pendulum and the Eradiquake types of isolators. The latter is made of a flat plate slider mounted on a disk bearing fitted with orthogonally aligned urethane springs as restoring force elements. It was stated that the Eradiquake system were utilized more than 20% of the North American Highway Bridges.

Jeong et al. (2016) developed a damper by using the sliding friction of aramid brake lining. The restoring capability of the device is supplied by pre-compressed polyurethane springs. The behavior of the damper closely matched flag-shaped behavior, resulting in self-centering and energy dissipation capacity.

Falborski and Jankowski (2017) reported results of an investigation on the effectiveness of a prototype base isolation system made of polymeric bearings. It was used specially prepared polymeric material with improved damping properties. Dynamic behaviors of single-story and two-story models, both fixed-base and base-isolated, under a number of different ground motions, were extensively studied. The peak accelerations recorded at the top demonstrated that application of the prototype polymeric bearings leads to significant improvement in seismic response. In addition, they stated that polyurethane spring has relatively high damping potential, which are crucial for the materials used for seismic isolation bearings.

Lihong et al. (2014) searched the judgment methods and threshold values of life assessment of marine vibration isolators. Aging and fatigue properties of rubber and polyurethane materials and their fatigue life were compared through the accelerated test method. Aging life of rubber (r) and polyurethane (p) materials at temperatures of 23 °C, 40 °C and 60 °C were determined as ($r=8.19$, $p=104.23$), ($r=1.24$, $p=18.13$) and ($r=0.27$, $p=4.5$) years, respectively. The results pointed out that polyurethane has substantial advantage

against rubber in terms of aging life. Dynamic fatigue performances of the two materials were tested in conditions of 20% initial strain, frequency of 10 Hz and amplitude of 1.27 mm. The polyurethane specimen was free from obvious appearance change after 1,000,000 cycles while surface of rubber material cracks after 500,000 cycles. They judged that the fatigue life of polyurethane material is more than 2 times of rubber material. Decrements in dynamic stiffness after 1,000,000 cycles were 5% and 18% for polyurethane and rubber specimens, respectively. Dependently, it was concluded that life of polyurethane vibration isolator is 2–3 times longer than rubber vibration isolator. When the temperature increases, polyurethane advantages in terms of aging life was more obvious compared to ordinary rubber.

Davies and Evrard (2007) performed an experimental study in which polyurethane samples with dissimilar hardness were subjected to immersion in artificial seawater for periods up to 2 years at temperatures from 50 to 100 °C. The similar samples were also immersed at sea for up to 5 years. The mechanical properties of the specimens were measured in tensile tests after ageing. The results from sea ageing confirmed that polyurethane samples retain 100% of their initial tensile properties after 5 years of immersion.

Clemitson (2015) provided data about the temperature effects on the behavior of polyurethane. The stiffness increases slowly from 20 °C to − 25 °C after which it increases rapidly. At these temperatures the hardness, tensile and tear strengths and torsional stiffness increases, also. Contrary, there is a gradual decrement in the properties above 80 °C. It was stated that polyurethane can be used with its initial properties between the temperature range of − 40 °C to 70 °C.

Falborski and Jankowski (2017) performed dynamic mechanical analyses to determine temperature effect and frequency rate of deformation on the response of polyurethane springs. The tests demonstrated that in typical atmospheric temperature range (− 20° to 40 °C) and for predominant earthquake frequencies (1–10 Hz), dynamic mechanical properties of polyurethane springs vary only slightly with changes in temperature and excitation frequency.

In this paper, a low-cost *polyurethane seismic isolation device* (PSID) is introduced. PSID consists of four polyurethane springs and two steel plates connected each other by a traded rod. The device is able to generate large elastic rotations associated with the limited lateral displacement. Hence, predominant vibrational period of post insulator supported by PSID is elongated and some extent of supplementary damping is generated. It satisfies the criteria defined by IEEE-693. The preliminary test results of PSID can be found elsewhere (Gokce et al. 2017). 550 kV post insulators were tested for fixed and isolated base conditions in the laboratory by using quasi-static and dynamic testing techniques.

2 Description of PSID and test specimen

The polyurethane springs used in PSID have 80 mm diameter and 125 mm height, respectively. The uniaxial compression tests were performed on the springs by using the testing setup shown in Fig. 2a. The typical axial force versus displacement relation presented in Fig. 2b were obtained. The maximum displacement was 32 mm (30% strain level) that was defined as elastic deformation limit. Shape of the force–displacement curve designates that the material has inherent damping property.

PSID consists of four polyurethane springs that are positioned between two circular stainless steel plates. Corrosion of stainless steel is typically limited following several

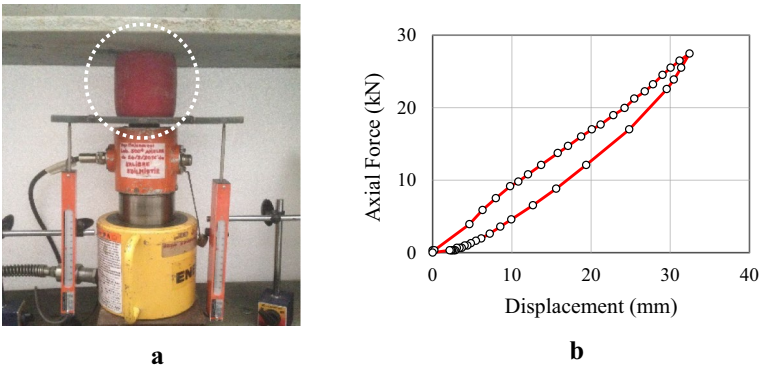

Fig. 2 Testing setup and force–displacement relation of the polyurethane spring. **a** Testing setup, **b** force–displacement relation

years of service, (Clemitson 2015). The plates are connected each other by pre-stressed steel rod (M14 bolt, 12.9 quality) positioned at their center. The springs are located in the cavities created on the steel plates. Depth of the cavities, which transfer shear forces between upper and lower steel plates, was selected as 7 mm depending on the preliminary calculations. Post-tension force applied to the rod was 70 kN. Thus, pre-compression load for each spring was 17.5 kN and it creates about 13% strain on them. Ten percent of tension strain is expected in the earthquake case, the remaining 3% is allocated to consider the possible long-term creep effect, (Buckle et al. 2006).

There are 8 holes on the steel plates of PSID to connect it to the supporting truss and cap of post insulator. The dimensions of PSID are given in Fig. 3.

A 550 kV post insulator was utilized in the experimental study with its iron made steel caps. Base and top core diameters were 180 mm and 150 mm, respectively. Total height of it was 4000 mm, Fig. 4. Self-weights of S_1, S_2 and S_3 posts were 1.43 kN, 1.49 kN and 1.46 kN, respectively. Eight M16 (8.8 quality) bolts were utilized for connection of the bottom insulator cap.

In the current practice of Turkey, porcelain insulators are supported on steel truss with varying geometry and stiffness properties. Independent suppliers provide the components. Dependently, the supporting truss is not accounted in design stage of porcelain insulator. PSID to be placed between steel truss and post insulator gives an occasion to

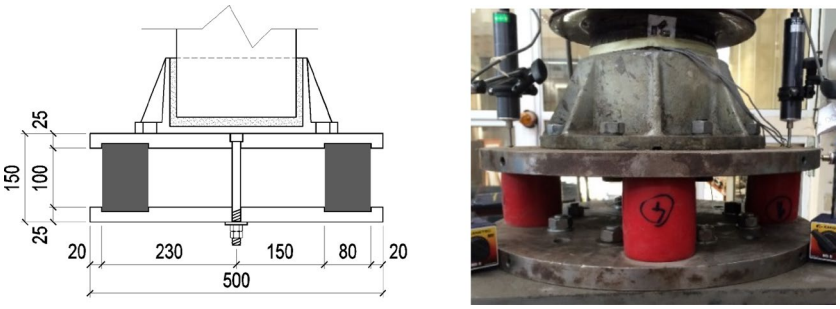

Fig. 3 Typical sectional dimensions (in mm) and photograph of PSID

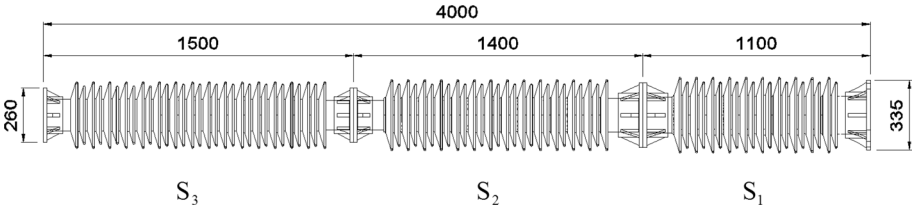

Fig. 4 Dimensions of the tested porcelain post insulator (in mm)

tune stiffness and damping properties of the system. The supporting truss used in the experimental study had plan dimensions of 500 × 500 mm and height of 900 mm. All members of the truss had L50.50.5 section. The steel plate with 20 mm thickness was welded top of the truss.

The post insulator system was evaluated theoretically for wind speeds of 36 m/s. Lateral top displacement arose from the wind effect was calculated as 35 mm that was rationally smaller than the expected displacement for strong earthquakes.

3 Experimental studies

3.1 Quasi-static tests of PSID

Quasi-static cyclic tests were performed to determine hysteretic behavior of PSID. Moment-rotation relation, stiffness variation, damping property are quantities extracted from the quasi-static tests. The loading pattern formed by the gradually increasing displacement targets was utilized in the tests, Fig. 5.

A steel column, 2.30 m in height, was utilized in the tests, Fig. 6. The column was laterally loaded by a servo-controlled MTS actuator.

Moment versus rotation relation of PSID obtained from the test is presented in Fig. 7. The base rotation was extracted from the vertical displacement measurements performed by a couple of transducer. The test was continued up to 0.045 rad. base rotation. Equivalent damping ratio determined from the procedure defined by Chopra (2001) is in the range of 4–8%.

Relative lateral displacement of PSID is presented in Fig. 8. The ultimate value was 3.3 mm that corresponds to 0.045 rad base rotation. No residual displacement was recorded in the quasi-static tests. It was resolved that PSID has large lateral stiffness compared with rotational flexibility.

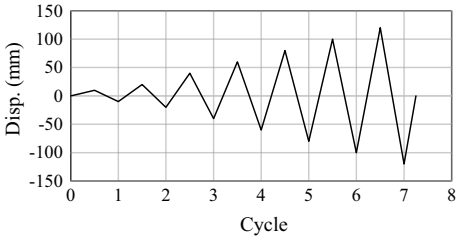

Fig. 5 Displacement pattern utilized in quasi-static cyclic tests

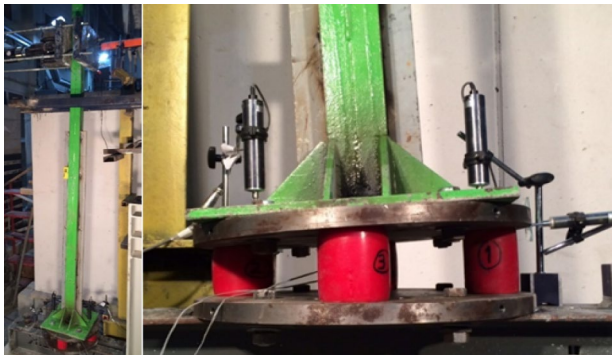

Fig. 6 Set-up utilized in quasi-static tests

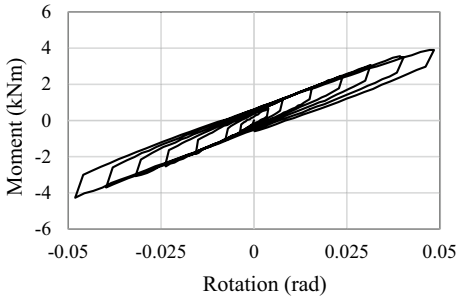

Fig. 7 Moment versus rotation relation of PSID

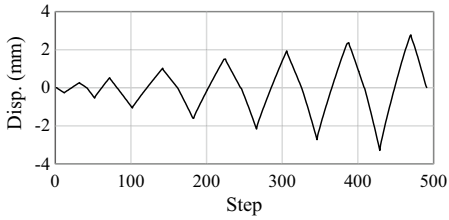

Fig. 8 Relative lateral displacement history of PSID

A few sinusoidal loading functions were applied to the specimen to evaluate the effect of loading rate. Because of the laboratory restraints, the loading rates varied in the range of 3–31 mm/s. The same path in base moment versus rotation relations was obtained.

3.2 Quasi-static tests of post insulator

Quasi-static cyclic tests were performed on the porcelain post insulators. Comprehensive information about the static tests can be found elsewhere, (Gokce et al. 2018). The specimen consists of two segments, Fig. 9. The bottom and top posts are 1.1 m and 1.4 m in heights, respectively. Solid core diameters decrease from bottom to top and diameters are $D_1 = 180$ mm, $D_2 = 160$ mm and $D_3 = 140$ mm. The specimen was rigidly connected to a steel beam at the bottom. A servo controlled MTS actuator was attached to the specimen.

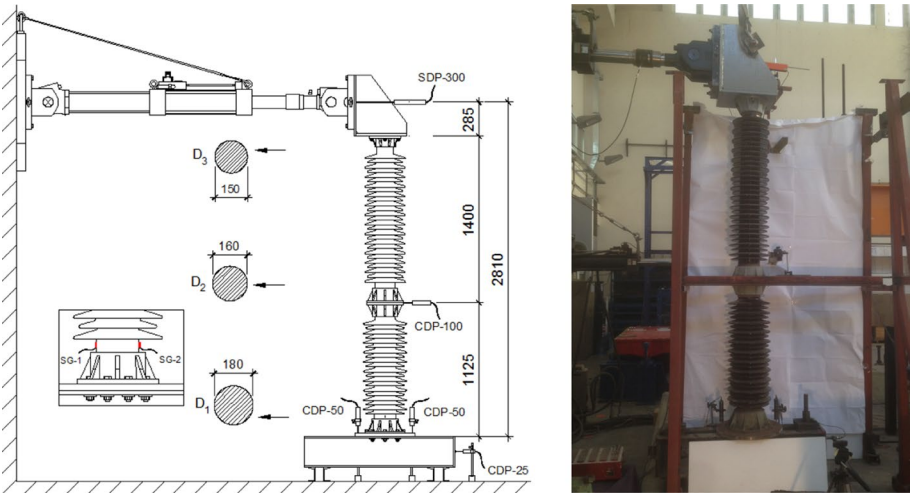

Fig. 9 Static test set-up for post insulators

Lateral displacements of the specimen were measured at neighborhood of D_1, D_2 and D_3 sections. Strain gauges measured longitudinal strains at the bottom section.

The displacement pattern that consists of ten distinct displacement targets was utilized, Fig. 10. Each displacement target was repeated two times, FEMA 461 (2007).

The experimental top displacement versus actuator force hysteresis is given in Fig. 11a. Maximum displacement and corresponding shear force capacity were 48.15 mm and 14.10 kN, respectively. Results of the strain measurements are found in Fig. 11b. The longitudinal strains measured at the opposite faces of the cross-section were almost symmetrical. The ultimate strain was recorded as 515 micro-strain.

Some cracks developed on cement-based grout placed between end cap and solid core of the insulator. The cracks were more serious at the middle connection (D_2). Henceforth, collapse initiated from the middle connection (D_2) (Fig. 12).

The lateral displacement distribution is sketched in Fig. 13 for 36.30 mm top displacement target. The value consists of two portions: $\delta_1 = 24.41$ mm and $\delta_2 = 11.89$ mm. The second portion (δ_2) is related with the connection flexibility of section D_2.

The longitudinal stresses are calculated at sections D_1 and D_2 by using the consistent bending moments. The bending moments corresponding to failure load were calculated as $M_i = 14.10$ kN$\times h_i$ where h_i is distance between actuator centerline and *ith* section. The stresses are calculated as $\sigma_1 = 65.38$ MPa and $\sigma_2 = 54.58$ MPa for D_1 and D_2 sections,

Fig. 10 Cyclic load pattern

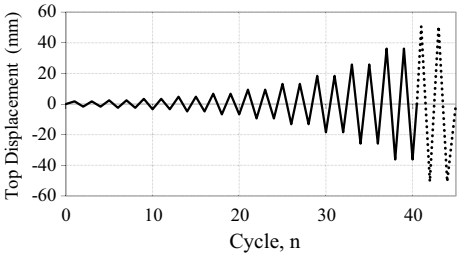

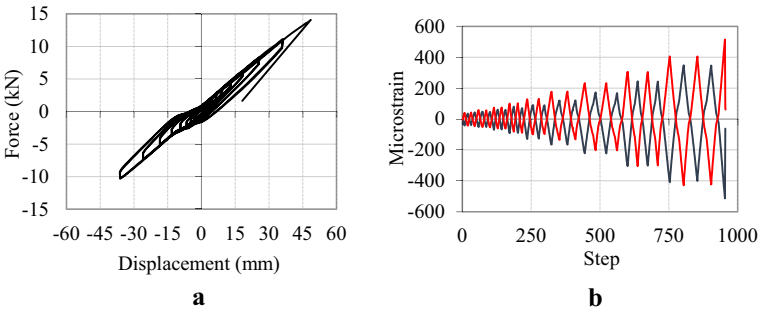

Fig. 11 Force versus displacement hysteresis and strain gauge measurements at section D_1. **a** Force–displacement history, **b** strain gauge measurements

Fig. 12 The failure mechanism

Fig. 13 Displacement distribution of the specimen

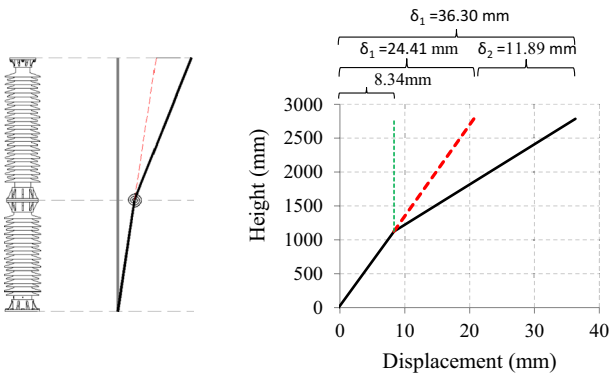

Fig. 14 Post insulator system on shake table

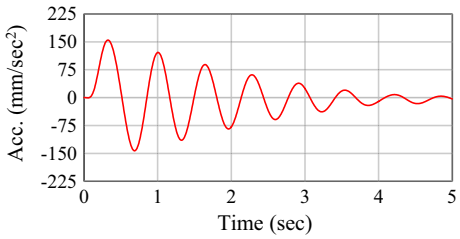

Fig. 15 Impact hammer test result of the isolated system

respectively. Although stress intensity in section D_1 is greater than section D_2, the collapse was initiated from section D_2. It may be attributed to the accumulated grout damages at the middle connection (D_2).

3.3 Free vibration tests

Two sovereign methods, namely impact hammer and pullback test were applied to determine free vibration characteristics of the fixed base and isolated systems. Pullback tests were performed for four different displacement intensities. Accelerometers were placed at top and bottom sections of post insulator, and top of supporting truss, Fig. 14.

The recorded typical data is presented in Fig. 15. Fundamental frequencies of the isolated and fixed base systems were obtained as 1.56 Hz and 5.57 Hz, respectively.

Two percent damping ratio was obtained for fixed base system. In the isolated system, damping ratio correlated with the applied displacement intensity. Details of damping tests for the isolated case is given in Table 1. The ratio varies in the range of 3–8% for the isolated case.

3.4 Strong ground motion data

Institute for Electrical and Electronics Engineers proposed acceleration spectra for seismic testing and qualification of substation equipment, IEEE-693. The acceleration spectra corresponding to *2% damped high performance level* were utilized in this

Table 1 Damping ratios obtained for the isolated case

Method	Top Disp. (mm)	Max. Acc. (mm/sn^2)	Fund. Freq. (Hz)	Damping ratio	
				Logarithmic decrement M. (%)	Half-power bandwidth M. (%)
Hammer T.	1.57	153	1.56	8.36	7.05
Pullback-F	25.12	1573	1.56	3.35	3.21
Pullback-2F	52.77	1380	1.56	4.87	3.94
Pullback-3F	88.14	4511	1.46	5.59	3.94
Pullback-4F	126.84	5040	1.46	6.00	3.90

Table 2 Selected earthquake data

Year	Earthquake	Station	M_w	PGA (mm/sn^2)	PGV (mm/sn)	PGD (mm)	Scale factor (SF)
1976	FRIULI	A-TMZ270	6.5	3088.3	308.0	50.9	1.84
1994	NORTHR	LOS270	6.7	4728.4	449.1	125.4	1.35
1987	SUPERST	B-POE360	6.5	2945.9	327.8	112.6	2.26
1989	LOMAP	CAP090	6.9	4348.7	292.2	54.9	1.63
1989	LOMAP	G03000	6.9	5444.8	356.8	82.6	1.65

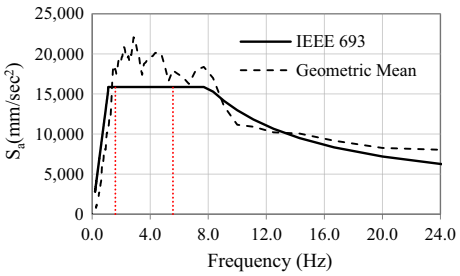

Fig. 16 IEEE-693 target spectrum versus mean spectrum of the selected records

study. Five historical acceleration records were selected from FEMA-P695 (2009) database. The important features of the records are listed in Table 2.

Fundamental vibrational frequencies of the tested fixed base and isolated specimens were 5.57 Hz and 1.56 Hz, respectively. The scaling procedure defined by Koliou et al. (2009) was applied to all acceleration data to fit their elastic spectra to the target one in the frequency range of 1.0–7.0 Hz. The scaling factors were obtained in the range of 1.35–2.26. They are listed in the last column of Table 1. Mean spectrum of the records is presented together with the target spectrum in Fig. 16. The critical frequencies of 5.57 Hz and 1.56 Hz are also revealed in the same figure. It is obvious that the mean spectrum is higher than the target one for the tested specimens.

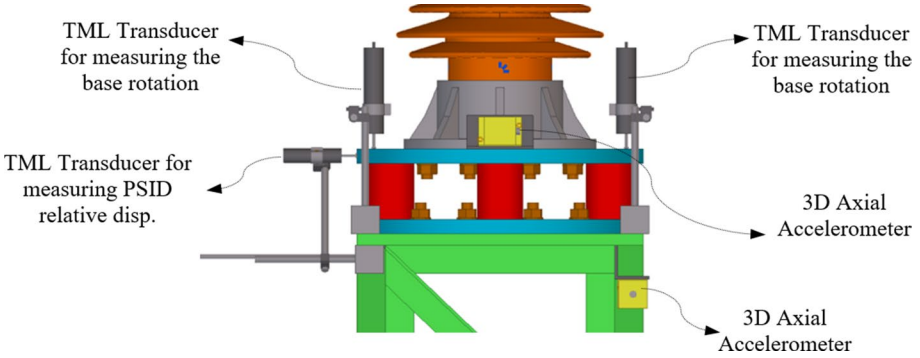

Fig. 17 The measuring system

Table 3 Comparison of the maximum top acceleration

Earthquake	Station	Fixed base (mm/s^2)	Isolated (mm/s^2)	Attenuation ratio (%)
FRIULI	A-TMZ270	11,534	9306	20
NORTHR	LOS270	17,980	11,187	38
SUPERST	B-POE360	16,429	9648	41
LOMAP	CAP090	13,341	10,266	23
LOMAP	G03000	25,134	9668	62

3.5 Shake table tests

The tests were performed on the uniaxial shake table facility of STEELab. Displacement capacity of the table is ± 325 mm, Fig. 10. 550 kV post insulator was positioned at center of the table. Measuring system comprises four accelerometers, three long- and three short-stroke displacement transducers, Fig. 17.

The acceleration records listed in Table 1 were employed in the shake table tests. The multipliers used to scale the records were 0.33, 0.66, 1.00 and (SF) given in Table 1. White noise tests were performed between the successive runs. The fixed base and isolated specimens completed all runs without any damage.

The measured top accelerations are compared in Table 3. PSID is effective to decrease accelerations in ratios of 20–70%.

Elastic acceleration spectra of the records for 2% damping ratio are presented in Fig. 18. The fundamental periods of isolated (T = 1/1.56 = 0.64 s) and fixed base (T = 1/5.56 = 0.18 s) specimens are also indicated in the figures. Spectral accelerations corresponding to the fundamental periods are gathered in Table 4.

The period elongation due to PSID caused higher spectral accelerations for FRIULI, NORTHR, LOMAP-CAP090 records. To reach more effectiveness, PSID should be designed with a fundamental frequency of 0.80 Hz or smaller.

Relative top displacement and absolute top acceleration histories for the selected earthquakes are presented in Figs. 19 and 20. They characterize the least and the most

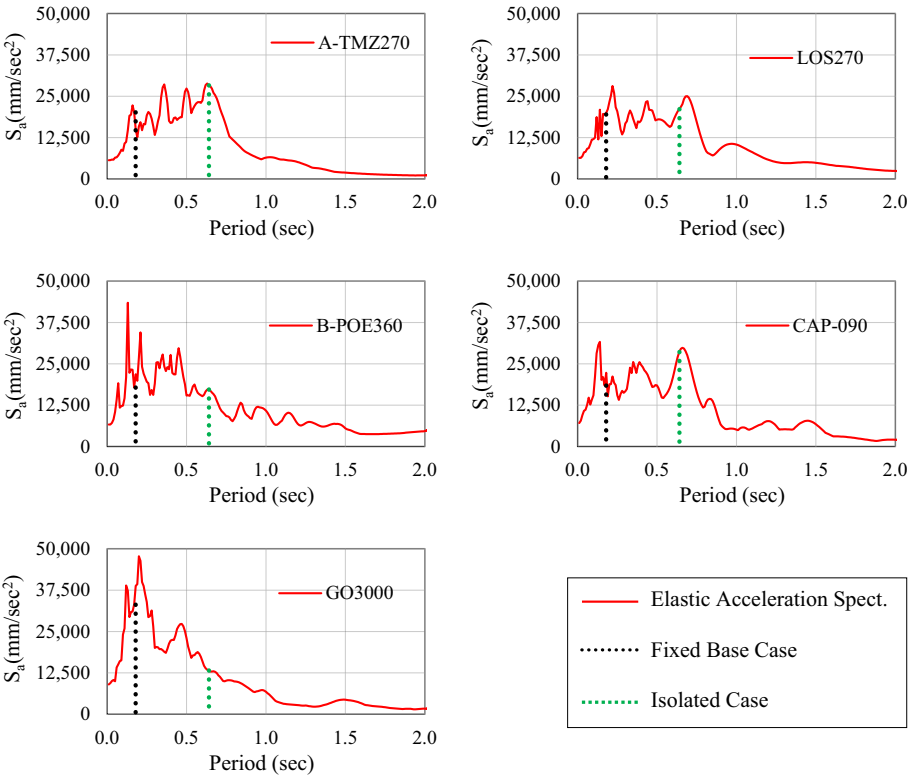

Fig. 18 Elastic acceleration spectra of the selected records

Table 4 Spectral acceleration ratios

Earthquake (1)	Station (2)	Fixed base (mm/s^2) (3)	Isolated (mm/s^2) (4)	Ratio (%) (4–3)/3
FRIULI	A-TMZ270	20,175	28,313	40
NORTHR	LOS270	19,547	21,112	8
SUPERST	B-POE360	17,862	17,271	−3
LOMAP	CAP090	18,451	28,578	55
LOMAP	G03000	33,138	13,224	−60

effective cases for PSID. Effectiveness ratios were calculated in Fig. 20. The recorded maximum top displacement was 183 mm.

When the top displacement is larger than the expectation, the isolated equipment requests some modification of its connections to cables to be able to accommodate the displacement demand. Usually these types of modifications are implemented by the utility companies. There are many examples of successfully modifying connections to accommodate large displacements of over 300 mm in the seismically isolated transformers, (Oikonomou et al. 2016; Stearns and Filiatrault 2005).

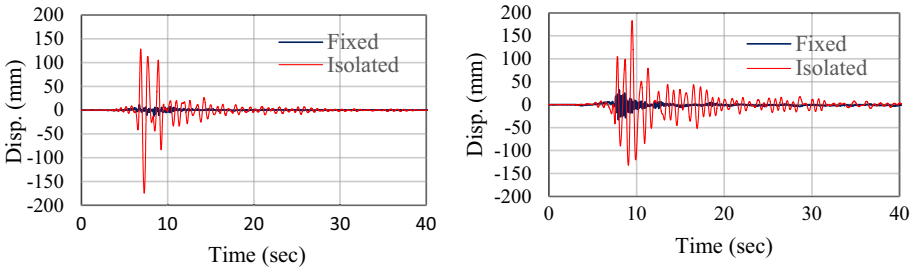

Fig. 19 The relative top displacement comparisons. **a** ATMZ-270, **b** GO-3000

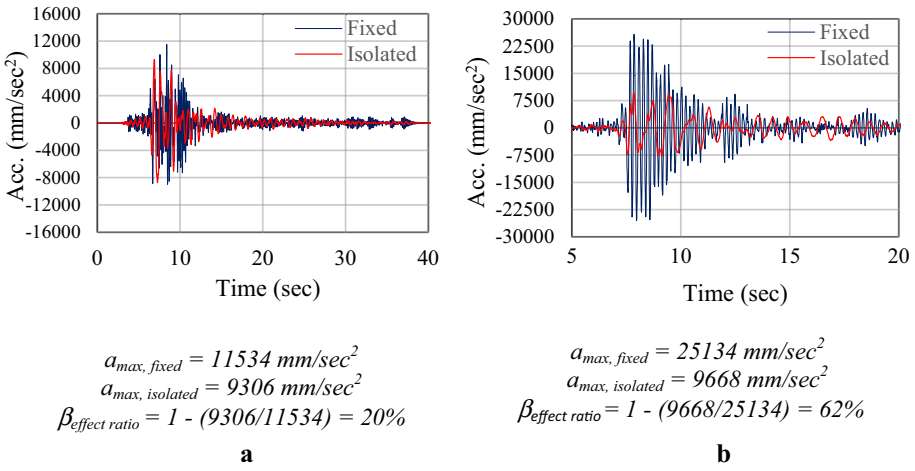

Fig. 20 The top absolute acceleration comparisons. **a** ATMZ-270, **b** GO-3000

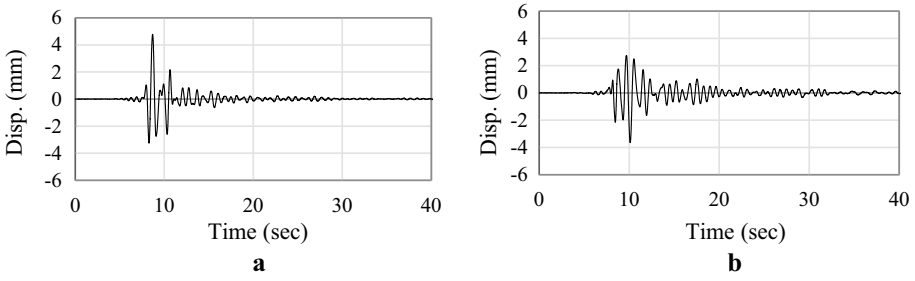

Fig. 21 The relative lateral displacement of PSID. **a** ATMZ-270, **b** GO-3000

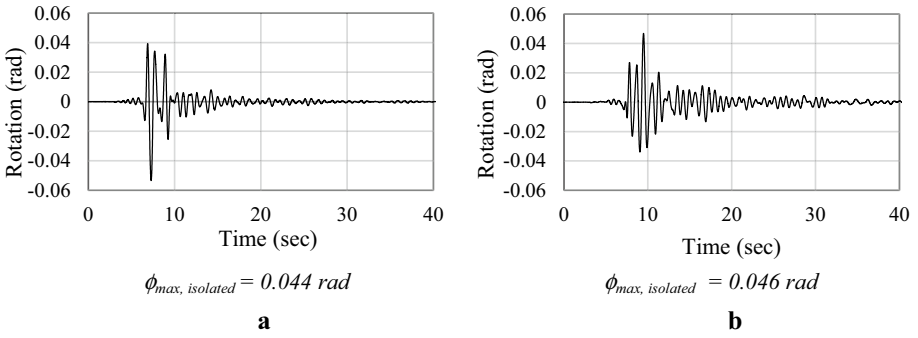

Fig. 22 PSID rotations. **a** ATMZ-270, **b** GO-3000

Relative lateral displacement and rotation histories of PSID for ATMZ-270 and GO3000 are given in Figs. 21 and 22.

Maximum relative lateral displacement of PSID was about 4.5 mm where relative top displacement was 183 mm. The measured maximum PSID rotation was about 0.05 rad and it corresponds to 65% of rotation capacity of the device. No residual rotation was recorded in the tests. PSID displayed self-centered response.

The experimental shear (V_b) and moment (M_b) histories at the bottom section of post insulator were determined through the recorded acceleration data, mass and height properties of the specimen. Formulae given by Koliou et al. (2009) were utilized for this purpose, Eq. 1.

$$\begin{aligned} V_b &= \int_0^H m(z)\, a(z)\, dz + c(z)\, v(z)\, dz \\ M_b &= \int_0^H m(z)\, a(z)\, z\, dz + c(z)\, v(z)\, z\, dz \end{aligned} \tag{1}$$

where $m(z)$, $a(z)$, $c(z)$ and $v(z)$ are mass, acceleration, damping and velocity profiles along height (z) of the post insulator. Second term on right hand side of the equations are related with damping. By neglecting the effect of damping, Eqs. 2 and 3 were obtained, (Koliou et al. 2009), where

$$V_b = \frac{m_b H a_o}{6}\left[\left(2\frac{a_b}{a_o}+1\right)+\frac{m_o}{m_b}\left(\frac{a_b}{a_o}+2\right)\right] \tag{2}$$

$$M_b = \frac{m_b H^2 a_o}{6}\left[\left(\frac{a_b}{a_o}+1\right)+\frac{m_o}{m_b}\left(\frac{a_b}{a_o}+3\right)\right] \tag{3}$$

(m_b, m_o) and (a_b, a_o) are mass and acceleration at bottom and top sections of post insulator. H stands for total height of post insulator.

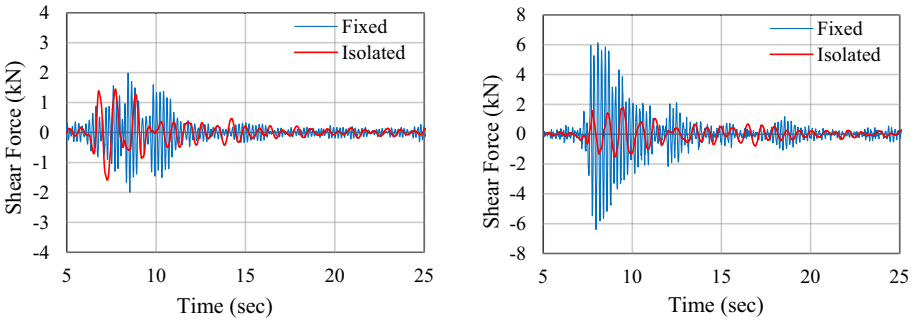

$V_{max,\ fixed} = 1.89\ kN$
$V_{max,\ isolated} = 1.59\ kN$
$\beta_{effect\ ratio} = 1 - (1.59/1.89) = 16\%$

a

$V_{max,\ fixed} = 6.42\ kN$
$V_{max,\ isolated} = 1.78\ kN$
$\beta_{effect\ ratio} = 1 - (1.78/6.42) = 72\%$

b

Fig. 23 Shear force histories. **a** ATMZ-270, **b** GO-3000

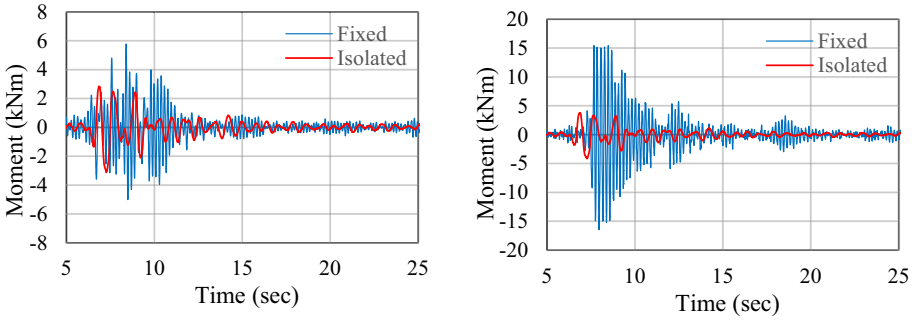

$M_{max,\ fixed} = 5.78\ kNm$
$M_{max,\ isolated} = 3.81\ kNm$
$\beta_{effect\ ratio} = 1 - (3.81/5.78) = 34\%$

a

$M_{max,\ fixed} = 15.43\ kNm$
$M_{max,\ isolated} = 3.33\ kNm$
$\beta_{effect\ ratio} = 1 - (3.33/15.43) = 78\%$

b

Fig. 24 Base moment histories. **a** ATMZ-270, **b** GO-3000

Table 5 Comparisons of the maximum base moment

Earthquake	Station	Fixed Base (kNm)	Isolated (kNm)	Effectiveness ratio (%)
(1)	(2)	(3)	(4)	(4–3)/3
FRIULI	A-TMZ270	5.78	3.81	34
NORTHR	LOS270	8.09	4.50	46
SUPERST	B-POE360	7.33	3.99	46
LOMAP	CAP090	5.56	3.98	28
LOMAP	G03000	15.43	3.33	78

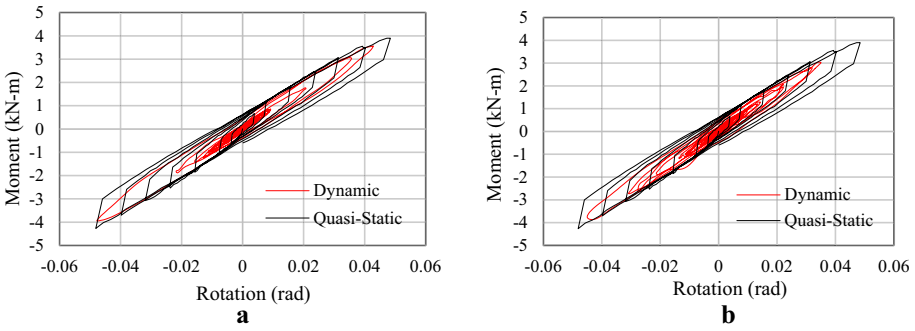

Fig. 25 Experimental moment-rotation relations of PSID. **a** ATMZ-270, **b** GO-3000

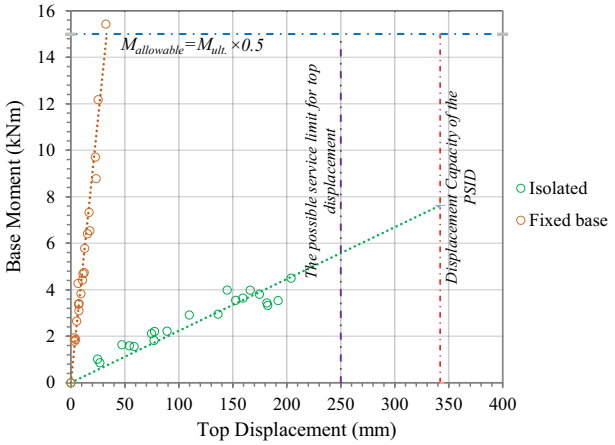

Fig. 26 Base moment versus top displacement relation of fixed base and isolated specimen

The experimentally obtained shear force and base moment histories are illustrated in Figs. 23 and 24 for ATMZ-270 and GO-3000. The effectiveness ratios are demonstrated in figures.

Ultimate moment capacity of post insulator was determined as $M_u = 39.5$ kN m from the performed quasi-static tests (Gokce et al. 2018). The capacity is above the obtained moments from shake table tests. Thus, no damage was observed in the tests. However, the latest versions of IEEE-693 (1985, 2006) suggested the allowable bending moment as $M_{all} = 0.25 \times M_u$ and $M_{all} = 0.50 \times M_u$, respectively. The base moments given in Table 5 are comparable with M_{all}. Moreover, the lower damage thresholds were suggested by Mohammadpour and Hosseini (2017) for assessment of the existing substation equipment that are relatively old and had poor engineering service.

Effectiveness ratios in terms of base moment are calculated in last column of Table 5. The minimum and maximum ratios are 28% and 78%, respectively. The inherent damping of PSID is apparent cause of the decrements for A-TMZ270, LOS270 and CAP090.

Base moment versus rotation hysteresis of PSID obtained from shake table and quasi-static tests are shown together in Fig. 25. Dynamic test results (PGV = 308 mm/s and 356 mm/s) are enclosed by the cycles of quasi-static test. It reveals that the effect of loading rate on the general response is limited.

Maximum top displacements and the corresponding base moments obtained from the shake table tests for the five acceleration records are presented in Fig. 26. Displacement capacity of the PSID and allowable base moment ($0.5 \times M_{ult}$) are also shown on the chart. The post insulator and PSID behave linear elastically until the defined limits. Reduction of the base moment for the specimen with PSID is seen obviously from Fig. 26. Furthermore, the possible service limit may be another critical restraint for the effective usage of the system.

3.6 Determination of structural damping through energy balance equation

The experimental data were utilized in determination of the terms of well-known energy balance equation, Eq. 4 (Akiyama 1985).

$$\int m\ddot{u}(t)\dot{u}(t)dt + \int c\dot{u}(t)\dot{u}(t)dt + \int f_s\dot{u}(t)dt = -\int m\ddot{u}_g(t)\dot{u}(t)dt \tag{4}$$

where m, c and f_s are mass, damping and restoring force matrices, respectively. $\ddot{u}$ and $\dot{u}$ are relative acceleration and velocity of the structure and $\ddot{u}_g$ is ground acceleration. Damping matrix c is rewritten as $c = 2\xi\omega$ where ξ is critical damping ratio and ω is circular frequency. Equation 5 is amended to the following form;

$$E_K + E_D + E_S = E_I \tag{5}$$

E_K, E_D, E_S are energy components and called as kinetic, damping and strain energies, respectively. E_I refers to total input energy imposed to the structure. An iterative procedure

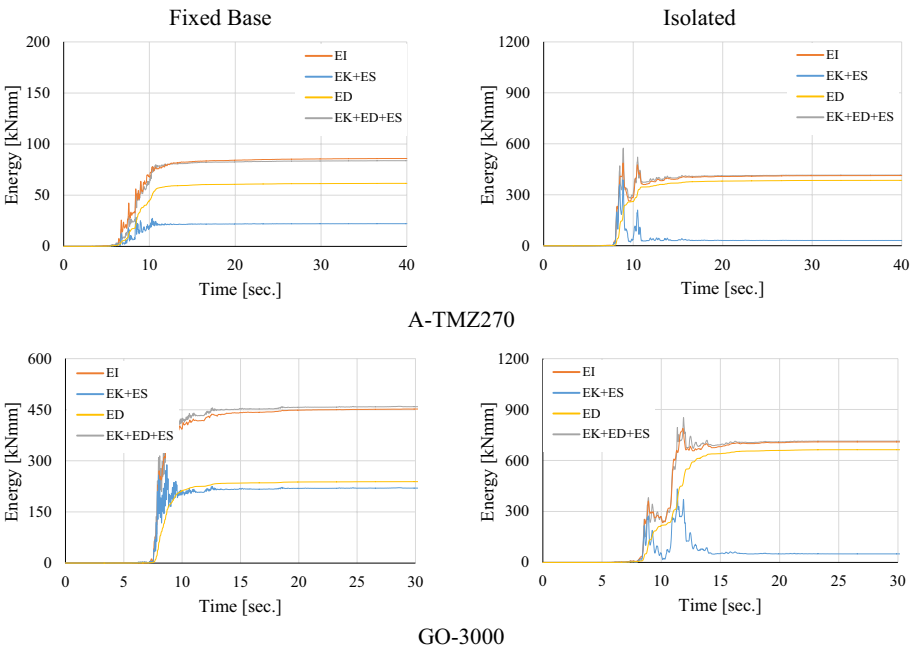

Fig. 27 The graphical representation of energy balance for shake table tests

Table 6 Structural damping ratios (ξ) determined by energy balance equation

Earthquake	Station	Fixed base (%)	Isolated (%)
FRIULI	A-TMZ270	2.2	5.0
NORTHR	LOS270	1.1	5.5
SUPERST	B-POE360	1.3	5.8
LOMAP	CAP090	1.8	5.3
LOMAP	G03000	0.8	5.1

was utilized to satisfy energy equilibrium. The explicit terms of E_K, E_S, E_I are calculated directly. E_D is determined through the assumption for ξ.

No inelastic deformations were observed on the specimen; so, f_s is elastic spring force. Graphical representation of the experimental energy equilibrium are illustrated in Fig. 27.

The calculated damping ratios (ξ) are collected in Table 6. Although, $\xi = 0.8 - 2.0\%$ is attained for fixed base case, PSID increases the ratio to $\xi = 5.0 - 5.8\%$.

4 Numerical evaluation

Numerical models of the specimens were prepared in SeismoStruct (2016). The models consist of the members to represent steel support, PSID components and post insulator. The unique non-linear element in the model is steel rod that connects steel plates of PSID. All other members were represented by *Elastic Frame Elements* depending on the experimental observations, Fig. 28a.

The mass and stiffness properties of the porcelain post insulator were directly determined from the measurements. Free vibration tests in discrete displacement ranges were

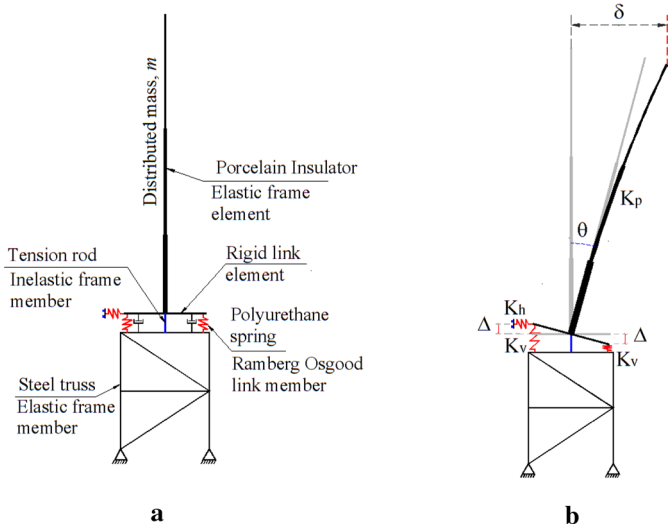

Fig. 28 The numerical model. **a** The components of numerical model, **b** representation of non-linear springs

performed to determine equivalent flexural stiffness ($E_{eqv} \times I$) of the post insulator system. It involves the effect of porcelain end connections. The lateral stiffness obtained from the failure tests executed for the post insulators are consistent with results of the free vibration tests. The discussion can be found elsewhere (Gokce et al. 2018).

Non-linear elastic behavior of polyurethane springs (K_v) was represented by Ramberg–Osgood model. Its parameters were defined as $F_y = 13.5$ kN, $\Delta_y = 0.007813$ m, $\gamma = 1.5$ depending on the experimental results, Sect. 3.1 and Fig. 28b. Relatively high shear resistance (K_h) was utilized for polyurethane springs.

Although 2% damping was consigned in fixed base case, 0.5% global damping was assigned for the isolated case. The inherent damping of PSID was represented through Ramberg–Osgood model. Non-linear time history analyses (NTHA) were performed by using Hilber–Huges–Taylor integration technique.

5 Comparison of numerical and experimental results

Absolute top acceleration comparison is presented here for fixed base case. Good correlation is observed between the experimental and numerical results, Fig. 29.

For the isolated case, several comparisons, i.e. absolute top acceleration, relative top displacement and base moment, are presented in Fig. 30.

In the comparison of absolute top accelerations, general forms of the curves are well-matched, but there are some discrepancies particularly for low amplitude peaks.

In the relative top displacement comparison, it is observed that main peaks are compatible but then again there are some disagreements for the succeeding peaks.

Good correlation was obtained for the base moment that is most critical quantity for design of PSID and post insulator. The differences between the experimental and numerical results were obtained in the range of 4–14%.

The numerical results are compared with the dynamic test results in terms of base moment versus rotation of the post insulator, Fig. 31. The cycles of two cases are consistent with each other.

The wide range acceleration spectra are generated at top of the specimen. Good correlation is obtained between the numerical and experimental results for the records, Fig. 32.

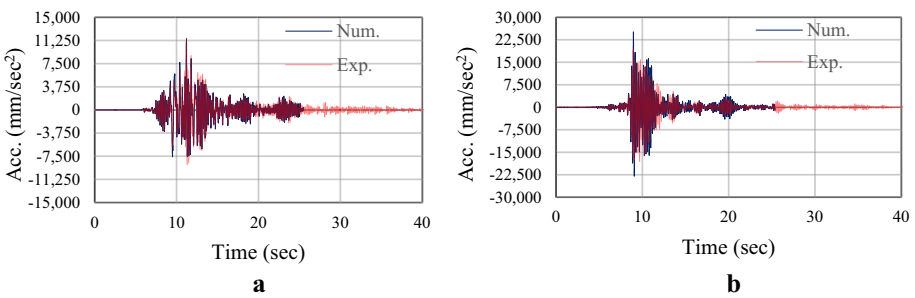

Fig. 29 Top acceleration comparisons for fixed base system. **a** ATMZ-270, **b** GO-3000

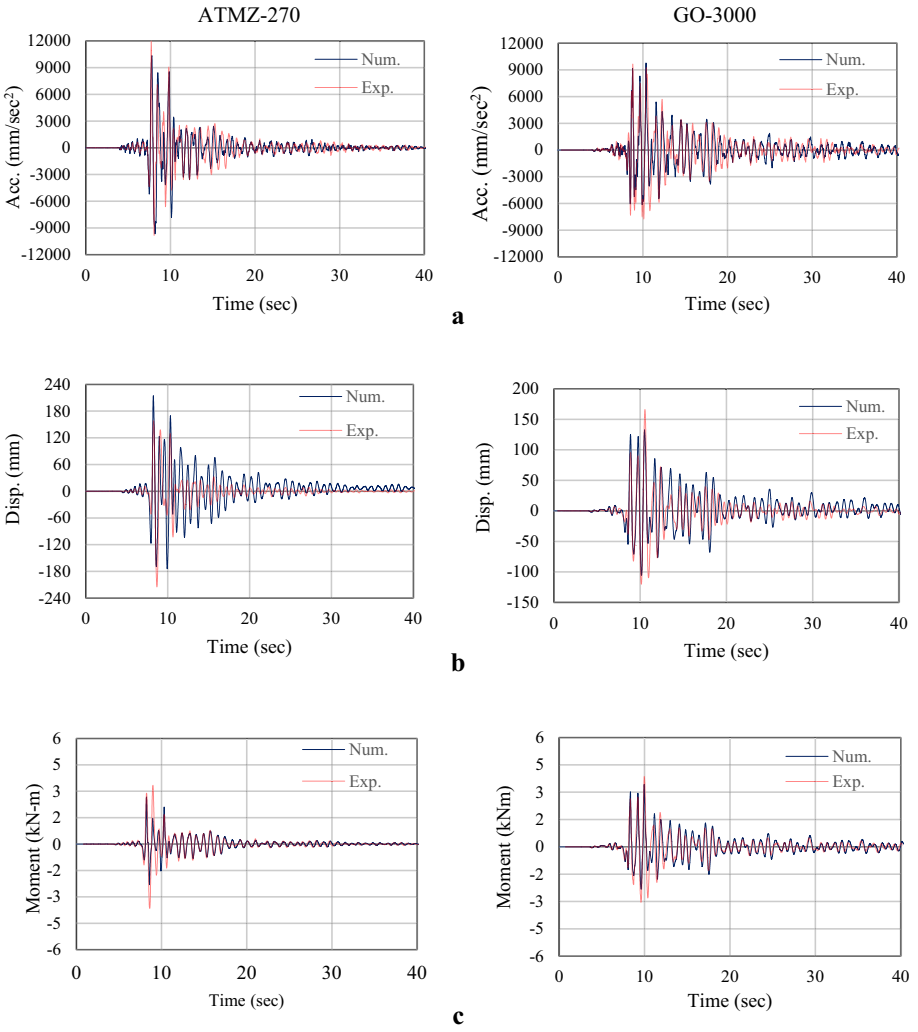

Fig. 30 Comparisons for the isolated system. **a** Absolute top acceleration, **b** relative top displacement, **c** base moment post insulator

6 Conclusions

A new cost-effective seismic isolation device for HV post insulators was developed and validated through the intensive experimental and numerical studies. The following conclusions can be driven.

- Significant seismic performance enhancement was obtained in terms of principal frequency, structural damping, shear force and bending moment intensities in post insulator.

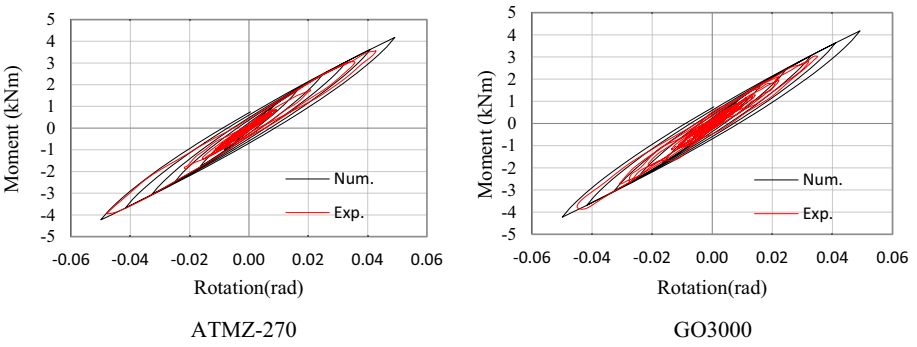

Fig. 31 Experimental versus numerical moment-rotation hysteresis of PSID

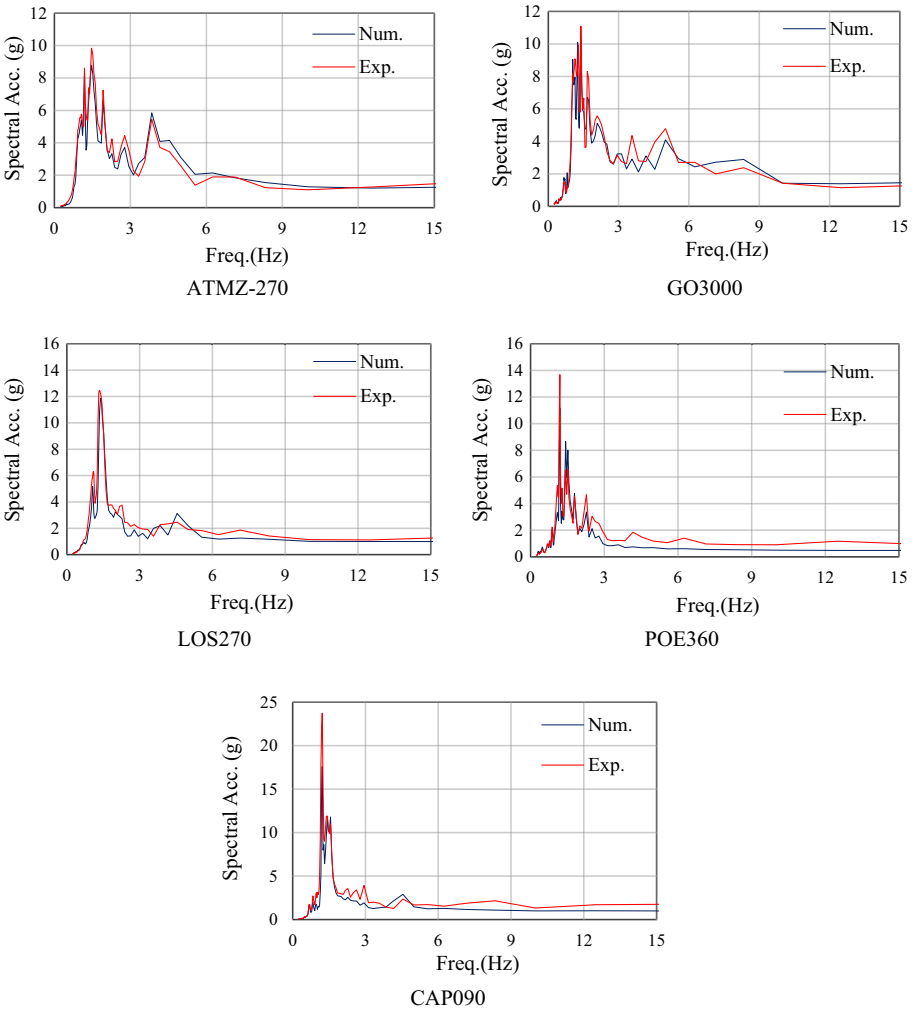

Fig. 32 Acceleration spectra at top of the specimen

- Fundamental periods (frequencies) were obtained as 0.18 s (5.57 Hz) and 0.64 s (1.56 Hz) for fixed base and isolated specimens, respectively. The rising of predominant period may improve the effectiveness of PSID. However, it should be noted that excessive increment of top displacement because of PSID flexibility would cause some trouble about the functionality of the post insulator.
- Equivalent viscous damping ratio extracted from the distinct testing methods for the system with PSID was in the range of 3–8% while it was 1–2% for fixed base system.
- Varying effectiveness ratios that are between 20 and 70% for top acceleration were obtained in the shake table tests. For more effective design of PSID, dominant frequency of the system can be made lower than 0.8 Hz.
- Base moment of the isolated system that is a crucial parameter in the seismic design reduced about 30–80% comparing with fixed base case.
- Maximum top displacement of the isolated system was 183 mm. The larger top displacement matter may cause some modifications in the cable connections of the seismically isolated device. Usually these modifications are implemented by the utility companies.
- The experimental results were replicated by the generated numerical models. Reasonable agreements were achieved for top acceleration, top displacement, shear force and bending moment of post insulator.

Acknowledgements The first author was sponsored by Bideb 2211 Program of Scientific and Technological Research Council of Turkey (TUBITAK). The study was sponsored by the research funds of Istanbul Technical University (ITU BAP 39552). 550 kV HV post insulators were supplied by Güral Electric Company. The study was carried out in the Structural and Earthquake Engineering Laboratory (STEELab) of ITU. All supports are gratefully acknowledged.

References

Akiyama H (1985) Earthquake-resistant limit-state design for buildings. University of Tokyo Press, Tokyo

Alessandri S, Giannini R, Paolacci F, Malena M (2015a) Seismic retrofitting of an HV circuit breaker using base isolation with wire rope. Part 1: preliminary test and analyses. Eng Struct 98:251–262

Alessandri S, Giannini R, Paolacci F, Malena M (2015b) Seismic retrofitting of an HV circuit breaker using base isolation with wire rope. Part 2: shaking table test validation. Eng Struct 98:263–274

Buckle I, Constantinou M, Dicleli M, Ghasemi H (2006) Seismic isolation of highway bridges (Report No. MCEER-06-SP07), MCEER, University at Buffalo, NY

Chopra AK (2001) Dynamic of structures, theory and application to earthquake engineering, 4th edn. Prentice-Hall, Upper Saddle River

Clemitson IR (2015) Castable polyurethane elastomers. CRC Press, Boca Raton

Davies P, Evrard G (2007) Accelerated ageing of polyurethanes for marine applications. Polym Degrad Stab 92(8):1455–1464

Falborski T, Jankowski R (2017) Experimental study on effectiveness of a prototype seismic isolation system made of polymeric bearings. Appl Sci 7(8):808

FEMA 461 (2007) Interim testing protocols for determining the seismic performance characteristics of structural and non-structural components. Applied Technology Council, California

FEMA P-695, (2009) Quantification of building seismic performance factors. Applied Technology Council for the Federal Emergency Management Agency, Washington

Filiatrault A, Matt H (2006) Seismic response of high voltage electrical transformer-bushing systems. J Struct Eng 132–2:287–295

Gokce T, Yuksel E, Orakdogen E (2017) Seismic protection of high voltage bushings by using polyurethane springs. In: 16th world conference on earthquake engineering, Santiago, Chile, Paper no: 2381

Gokce T, Orakdogen E, Yuksel E (2018) Failure mode investigation for high voltage porcelain insulators. In: 16th European conference on earthquake engineering, Thessaloniki, Greece, Paper no: 11334

Hatami M, Ashtiany MG, Hosseini M (2004) Experimental and analytical study of a high voltage instrument transformer. In: 13th world conference on earthquake engineering, Vancouver, BC, Canada, Paper no: 2550

IEEE 693 (1985 & 2006) Recommended practice for seismic design of substations. IEEE Standard Department, Piscataway, NJ

Jeong K, Choi E, Back SY, Kang JW (2016) Smart damper using sliding friction of aramid brake lining and self-centering of rubber springs. Int J Steel Struct 16(4):1239–1250

Koliou M, Filiatrault A, Reinhorn AM (2009) Seismic protection of electrical transformer bushing systems by stiffening techniques (Report No. MCEER-12-002), MCEER, University at Buffalo, NY

Kong D, Reinhorn A (2009) Seismic evaluation and protection of high voltage disconnect switches. Lifeline earthquake engineering in a multihazard environment, ASCE, pp 221–231

Lee D, Constantinou MC (2018) Combined horizontal–vertical seismic isolation system for high voltage–power transformers: development, testing and validation. Bull Earthq Eng 16:4273–4296

Lihong S, Zhiqiang L, Xue Y (2014) Experimental study of marine polyurethane isolator life. In: The 21st international congress on sound and vibration. Beijing, China

Mohammadpour S, Hosseini M (2017) Experimental system identification of a 63 kV substation post insulator and the development of its fragility curves by dynamic finite element analyses. Earthq Spectra 33(3):1149–1172

Murota N, Feng MQ, Liu GY (2006) Earthquake simulator testing of base-isolated power transformers. IEEE Trans Power Delivery 21–3:1291–1299

Oikonomou K, Constantinou MC, Reinhorn AM, Leon K Jr (2016) Seismic isolation of high voltage electrical power transformers (Report No. MCEER 16-0006), MCEER, University at Buffalo, NY

Schiff A (1998) Guide to improved earthquake performance of electrical power systems (Report No. NIST GCR 98-757). National Institute for Standards and Testing, Washington, D.C

SeismoStruct (2006) A computer program for static and dynamic nonlinear analysis of framed structures. Pavia, Italy. Seismosoft http://www.seismosoft.com

Stearns C, Filiatrault A (2005) Electrical substation equipment interaction: experimental rigid conductor studies PEER Report 2004/09. Pacific Earthquake Engineering Research Center, College of Engineering University of California, Berkeley

Takhirov S, Fujisaki E, Kempner L, Riley M, Low B (2017) Full-scale component testing of seismic isolation devices and verification of their performance in full-scale system level tests on a shaking table. In: 7th international conference on advances in experimental structural engineering, Pavia, Italy

Villaverde R, Pardoen GC, Carnalla S (2001) Ground motion amplification at flange level of bushings mounted on electric substation transformers. Earthquake Eng Struct Dynam 30:621–632

Whittaker AS, Fenves GL, Gilani ASJ (2004) Earthquake performance of porcelain transformer bushings. Earthq Spectra 20:205–223